JUSTC

Article

http://justc.ustc.edu.cn

Received: April 23, 2022; Accepted: May 30, 2022

A deformable spinel-type chloride cathode with high ionic conductivity for all-solid-state Li batteries

Jipeng Hao, and Cheng Ma ✉

Department of Materials Science & Engineering, University of Science and Technology of China, Hefei 230026, China

✉Correspondence: Cheng Ma, E-mail: mach16@ustc.edu.cn

Graphical abstract

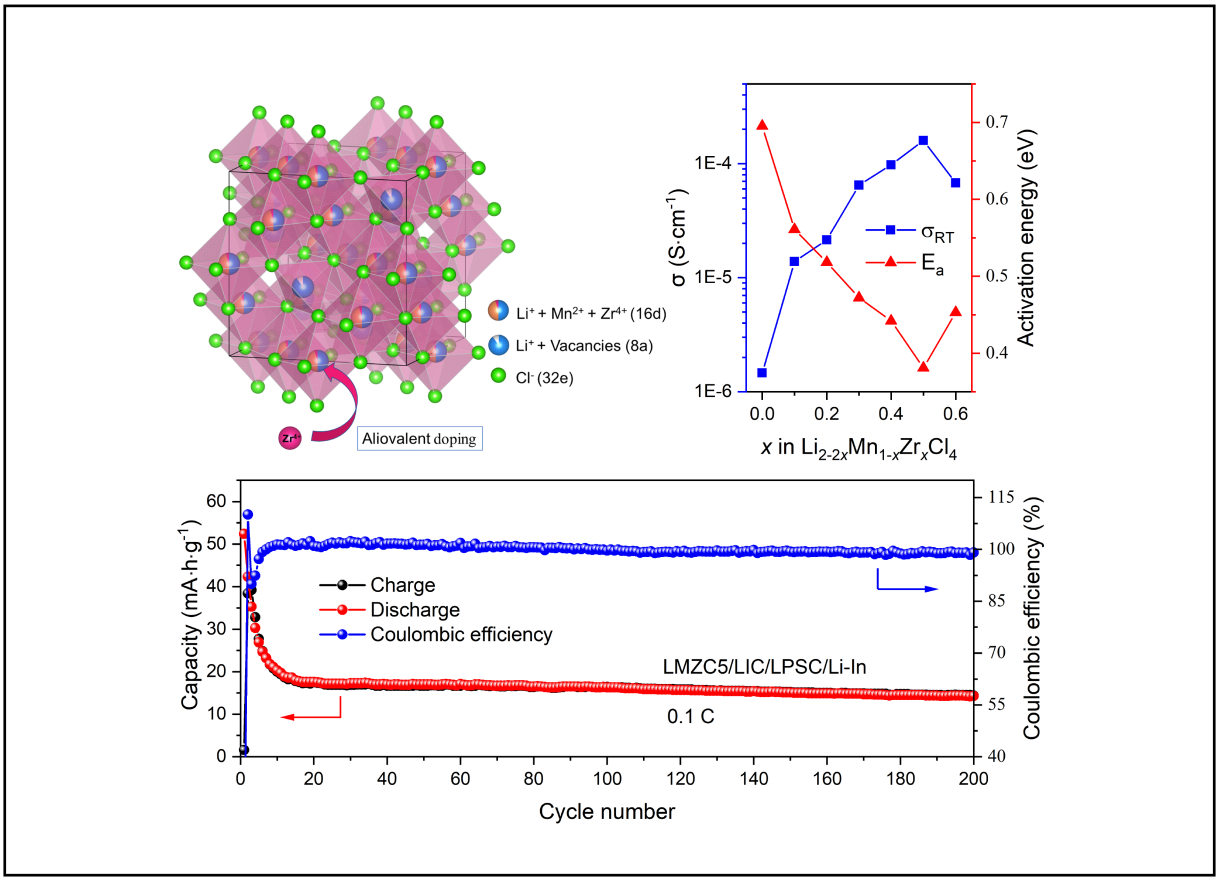

Zr^{4+}-doped spinel-type chloride $Li_{2-2x}Mn_{1-x}Zr_xCl_4$ exhibits high ionic conductivity and promising cycling stability.

Public summary

- A series of deformable spinel-type chloride cathodes $Li_{2-2x}Mn_{1-x}Zr_xCl_4$ were synthesized by mechanical ball milling.
- The Zr^{4+}-doped $Li_{2-2x}Mn_{1-x}Zr_xCl_4$ exhibits high ionic conductivity and low activation energy, which was confirmed by electrochemical impedance spectroscopy.
- The optimal composition $LiMn_{0.5}Zr_{0.5}Cl_4$ was integrated as the cathode into all-solid-state cells, and a promising cycling stability for 200 cycles was achieved.

Citation: Hao J P, Ma C. A deformable spinel-type chloride cathode with high ionic conductivity for all-solid-state Li batteries. *JUSTC*, **2022**, 52(12): 4. DOI: 10.52396/JUSTC-2022-0071

JUSTC

Article

http://justc.ustc.edu.cn

Received: April 23, 2022; Accepted: May 30, 2022

A deformable spinel-type chloride cathode with high ionic conductivity for all-solid-state Li batteries

Jipeng Hao, and Cheng Ma ✉

Department of Materials Science & Engineering, University of Science and Technology of China, Hefei 230026, China

✉Correspondence: Cheng Ma, E-mail: mach16@ustc.edu.cn

Cite This: *JUSTC*, **2022**, 52(12): 4 (7pp)

Read Online

Abstract: All-solid-state Li batteries (ASSLBs) are now considered to be next-generation energy storage devices due to their advantages in safety and energy density. With liquid electrolytes replaced by solid electrolytes, novel cathode active materials (CAMs) with different characteristics are needed. The solid-solid contact in ASSLBs requires CAMs to have good deformability. In addition, higher ionic conductivity is also essential to reduce the mass of the Li-ion conductive agent, thus accessing a higher overall capacity. Herein, we report a spinel-type chloride cathode $Li_{2-2x}Mn_{1-x}Zr_xCl_4$, which has good deformability and high ionic conductivity (up to 0.16 mS·cm^{-1} at 25 °C). The ASSLB using the optimal composition of $LiMn_{0.5}Zr_{0.5}Cl_4$ as the cathode exhibits promising cycling stability for 200 cycles at room temperature.

Keywords: all-solid-state Li batteries; cathode; ionic conductivity; deformability; spinel

CLC number: TQ131.1 **Document code:** A

1 Introduction

Recently, all-solid-state Li batteries (ASSLBs) have attracted great interest for their potential to offer higher energy density and better safety[1, 2]. However, the substitution of liquid-solid contact with solid-solid contacts brings significant challenges[3–5]. For example, the requirements for the cathodes in ASSLBs are no longer the same as those in commercial Li-ion batteries using liquid electrolytes.

The difference is at least twofold. On the one hand, insufficient contact between brittle, nondeformable solid particles would lead to high resistance for Li^+ transport. Therefore, to maintain good interfacial contact, cathode particles should preferably show good deformability[6]. On the other hand, to improve ionic diffusion in cathodes, the addition of SSEs (solid-state electrolytes) is usually needed in the composite cathode, but these electrochemically inert materials inevitably decrease the mass loading of active materials and thus the energy densities[7]. However, if the cathode itself is highly Li-ion conductive, the composite cathode would no longer need much solid electrolyte to make its ionic transport sufficiently fast. According to Gao et al.[5], the composite cathode of ASSLBs should have a high ionic conductivity of more than 10^{-4} S·cm^{-1}. Therefore, to decrease or eliminate the need for solid electrolytes in the composite cathode, the ionic conductivity of the cathode active material itself should at least reach this level. Unfortunately, realizing the two characteristics mentioned above (especially the deformability) in the present mainstream cathodes is rather difficult because they are all brittle, poorly deformable oxides[8, 9].

Chlorides have good deformability and high oxidation potential; in addition, their open structures can support good ionic conduction, giving them great potential as cathode materials. Most chlorides are soluble in polar solvents, so there is not much research on such electrode materials in the past[8]. The deformable spinel-type chloride $Li_2M^{II}Cl_4$ (M^{II} = Mn, Mg, Fe, Cd, V, Cr, etc.) may contain transition-metal cations and thus could potentially serve as the cathode. Among Li_2MCl_4-type chlorides, Li_2MnCl_4 has the highest Li^+ conductivity (4×10^{-6} S·cm^{-1}, 25 °C)[10], and the nonstoichiometric $Li_{2-2x}Mn_{1+x}Cl_4$ can reach 1.5×10^{-5} S·cm^{-1} [11], but still does not satisfy the requirements. To be a qualified cathode active material (CAM), it needs to be sufficiently conductive.

In this work, the aliovalent substitution $Li_{2-x}Mn_{1-x}Zr_xCl_4$ with high Li^+ conductivity (up to 1.60×10^{-4} S·cm^{-1}) was synthesized by mechanical ball milling, and the ionic conductivity and activation energy of the powder were investigated. Moreover, the remarkable reversibility of the all-solid-state Li-In/Li_6PS_5Cl-Li_3InCl_6/$LiMn_{0.5}Zr_{0.5}Cl_4$ cell over 200 cycles was demonstrated.

2 Materials and methods

2.1 Preparation of materials

All preparations were conducted under an Ar atmosphere. For the preparation of as-milled $Li_{2-2x}Mn_{1-x}Zr_xCl_4$, stoichiometric amounts of precursors LiCl (99.99%, Alfa Aesar), $MnCl_2$ (99.9%, Aladdin), and $ZrCl_4$ (98%, Alfa Aesar) were hand-mixed in the mortar by pestle for homogenization. Subsequently, the as-mixed stoichiometric mixture was mechanically milled at 500 r/min for 25 h in an 80 mL ZrO_2 vial with ZrO_2 balls (ϕ = 5 mm) using a PULVERISETTE 7 premium line (Fritsch GmbH), and the ball-to-powder weight ratio was 15∶1.

To obtain annealed samples, as-milled powder samples

DOI: 10.52396/JUSTC-2022-0071

JUSTC, **2022**, 52(12): 4

were sealed in a quartz ampoule under vacuum and then heat-treated at 350 °C for 5 h with a heating rate of 5 °C·min^{-1} and naturally cooled to room temperature. Li_3InCl_6 (LIC) was prepared by mechanical milling and subsequent heating treatment. A stoichiometric amount of LiCl (99.99%, Alfa Aesar) and $InCl_3$ (99.99%, Alfa Aesar) was milled under the same conditions as for $Li_{2-2x}Mn_{1+x}Cl_4$, which was followed by annealing at 350 °C for 5 h with Ar flow.

2.2 Material characterization

Powder X-ray diffraction (XRD) patterns were collected on a Rigaku Ultima IV diffractometer with Cu Kα1 radiation (λ = 1.54178 Å). Prior to the XRD measurements, the powder samples were sealed in Kapton film in an Ar-filled glovebox to avoid air exposure. The scanning speed was 10° per minute, and the scanning range was from 20° to 80°.

2.3 Conductivity measurements

Li^+ conductivity was measured by electrochemical impedance spectroscopy (EIS) on a BioLogic MTZ-35 impedance analyzer. Prior to the AC impedance spectroscopy measurements, the powders were cold pressed into pellets at 370 MPa, and then Au electrodes were sputtered on the pellet surfaces as blocking electrodes. The thickness of the pellet was between 0.6–0.8 mm. The above procedures were performed inside an Ar-filled glovebox to avoid air exposure. The frequency range of the EIS measurement was from 1 Hz to 35 MHz with a 50 mV driving potential amplitude. The electronic conductivity was determined by direct current (DC) polarization measurements on a Chenhua CHI630e. The cold-pressed pellets were measured at 25 °C with an applied voltage of 1 V.

2.4 Electrochemical characterization

All ASSLB preparation processes were performed inside an Ar-filled glove box. The cathode composite powder was prepared by mixing as-milled $LiMn_{0.5}Zr_{0.5}Cl_4$ (LMZC5) and an electron-conductive additive carbon nanotube (CNT) using a ball mill apparatus (Fritsch GmbH). The electrochemical stability window (ESW) was evaluated by linear sweep voltammetry (LSV) measurements on a Li/Li_6PS_5Cl-LMZC5/LMZC5+CNT (weight ratio: LMZC5/CNT = 70/30) semi-blocking cell[12]. To assemble an all-solid-state battery, approximately 40 mg LIC was added into a polyetheretherketone (PEEK) die with a diameter of 10 mm and cold pressed at 1 ton as the SSE layer. To avoid reaction between LIC and the Li-In anode, 50 mg Li_6PS_5Cl (Hefei Kejing, 99%) was further added and pressed at 1.5 tons. Then, 10 mg of the cathode composite powder was dispersed on the LIC side of the double-layer solid electrolyte and pressed again at 2 tons. Finally, a piece of indium foil (0.1 mm thick, 10 mm diameter) was placed at the surface of the Li_6PS_5Cl layer, and a piece of lithium foil (0.03 mm thick, 10 mm diameter) was then placed on the indium foil. The ASSLB was cycled under a stack pressure of 2 tons at 25 °C using a LAND CT2001A cycler within the potential window of 1.5–3.6 V (vs Li^+/LiIn).

3 Results and discussion

The X-ray diffraction (XRD) patterns of the as-milled $Li_{2-2x}Mn_{1-x}Zr_xCl_4$ (x = 0, 0.1, 0.2, 0.3, 0.4, 0.5, 0.6, abbreviated as LMC, LMZC1, LMZC2, LMZC3, LMZC4, LMZC5 and LMZC6, respectively) powder samples are shown in Fig. 1. In the range of $0 \leqslant x \leqslant 0.4$, the XRD patterns match well with Li_2MnCl_4 (ICSD No. 97-000-1984)[13]. The main characteristic peaks of the two components LMZC5 and LMZC6 are also consistent with Li_2MnCl_4, while a weak characteristic peak belonging to the Li_2ZrCl_6 impurity can be observed at approximately 32° in LMZC5. Further substitution of x = 0.6 resulted in more obvious peaks of Li_2ZrCl_6. The results indicate that the mutual solubility of Zr^{4+} in Li_2MnCl_4 should be between 0.4 and 0.5. In addition, it can be observed from Fig. 1b that with increasing doping ratio, the characteristic peak shifts to a high angle, which indicates that Zr^{4+} has been successfully doped into the structure of Li_2MnCl_4. Due to the smaller ionic radius of Zr^{4+} (compared to Mn^{2+}) and the generation of Li^+ vacancies, the lattice constant of the material decreases with increasing doping ratio.

The crystallinity of samples obtained by mechanical ball milling is very low, while previous studies have shown that for chloride solid electrolytes, the highly crystalline phases generally tend to have higher ionic conductivity[14, 15]. Therefore, the as-milled samples were annealed at 350 °C for 5 h to improve the crystallinity. The XRD patterns of the annealed samples are shown in Fig. 2. The main characteristic peaks are the same as before, while the intensities are much higher, and peaks with lower intensity that cannot be observed in the as-milled samples can also be clearly displayed, indicating that the annealing process greatly improved the crystallinity. In addition, no impurity peak was found in the annealed samples for all different doping ratios, which means that the annealed samples are all single-phase materials with Li_2MnCl_4 structures. As mentioned above, weak characteristic peaks of α-Li_2ZrCl_6 can be observed in the as-milled samples for LMZC5 and LMZC6, but peaks of the corresponding high-

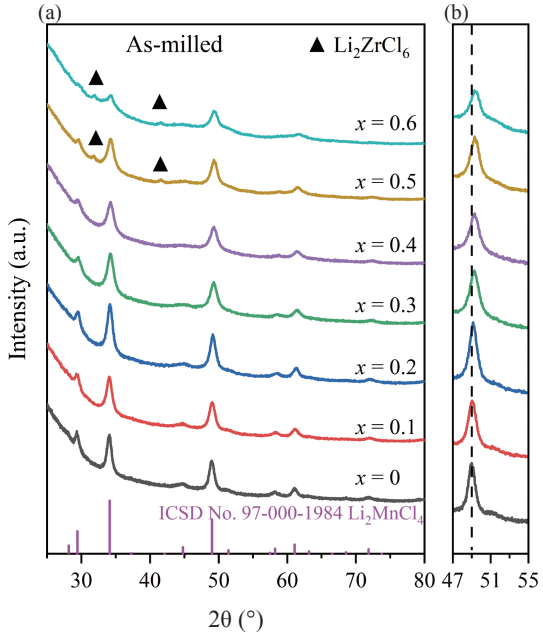

Fig. 1. (a) XRD patterns of as-milled $Li_{2-2x}Mn_{1-x}Zr_xCl_4$. (b) Partial enlarged image of (a).

DOI: 10.52396/JUSTC-2022-0071
JUSTC, **2022**, 52(12): 4

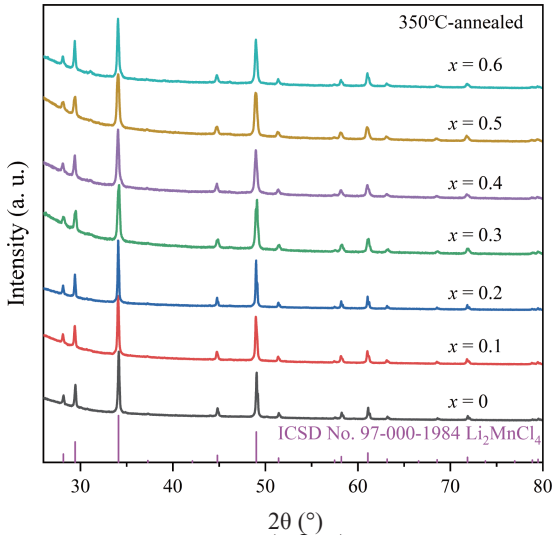

Fig. 2. XRD patterns of the 350 °C-annealed $Li_{2-2x}Mn_{1-x}Zr_xCl_4$ powder samples.

temperature phase (β-Li_2ZrCl_6)[16] were not found in the annealed samples. This phenomenon may be explained by the fact that the as-milled samples are in a metastable state, and after annealing, the structure is more stable; thus, the solid solubility of Zr^{4+} is improved.

Fig. 3a, b displays the typical Nyquist plots of the as-milled and annealed samples, respectively. The impedance spectra were fitted with the equivalent circuit consisting of one parallel constant phase element (CPE)/resistor (R) in series with another CPE. The low electronic conductivities of the as-milled and annealed samples were measured, as shown in Fig. 3c, d. The Li^+ conductivities and electronic conductivities of all samples are listed in Table 1, 2. With the aliovalent substitution of Zr^{4+}, the Li^+ conductivities of the as-milled samples can reach ~10^{-4} S·cm^{-1}. However, the Li^+ conductivity decreased by two orders of magnitude after annealing at 350 °C for 5 h. Since the Li^+ conductivities of the annealed samples are all on the order of 10^{-6} S·cm^{-1}, which cannot satisfy the requirements of assembling all-solid-state batteries, they will not be discussed in the following.

The Arrhenius plots derived from the Nyquist plots at different temperatures (Fig. 4a) showed good linearity. The ionic conductivities at 25 °C and activation energies (E_a) determined according to the Arrhenius equation of $Li_{2-2x}Mn_{1-x}Zr_xCl_4$ are shown in Fig. 4b. The ionic conductivities of the samples increase gradually with increasing Zr^{4+} substitution, while the E_a values gradually decrease with increasing Zr^{4+} content. The highest ionic conductivity (1.6×10^{-4} S·cm^{-1} at 25 °C) is achieved for $x = 0.5$, which also exhibits the lowest activation energy (0.381 eV). However, further substitution of $x = 0.6$ resulted in a decrease in the ionic conductivity. According to the previous XRD patterns, weak peaks of Li_2ZrCl_6 can be observed in LMZC5 and LMZC6. While the reported ionic conductivity of Li_2ZrCl_6 is higher (~4×10^{-4} S·cm^{-1})[17], it seems that the presence of Li_2ZrCl_6 in LMZC6 does not further improve its ionic conductivity. It could be reasonably inferred that the ionic conductivity of the sample is still mainly affected by the structural change of Li_2MnCl_4, and the content of Li_2ZrCl_6 is too low to have a significant impact on its ionic conductivity. Last but not least, it should be noted that all the conductivity measurements above were conducted directly on cold-pressed powders without any heat treatment.

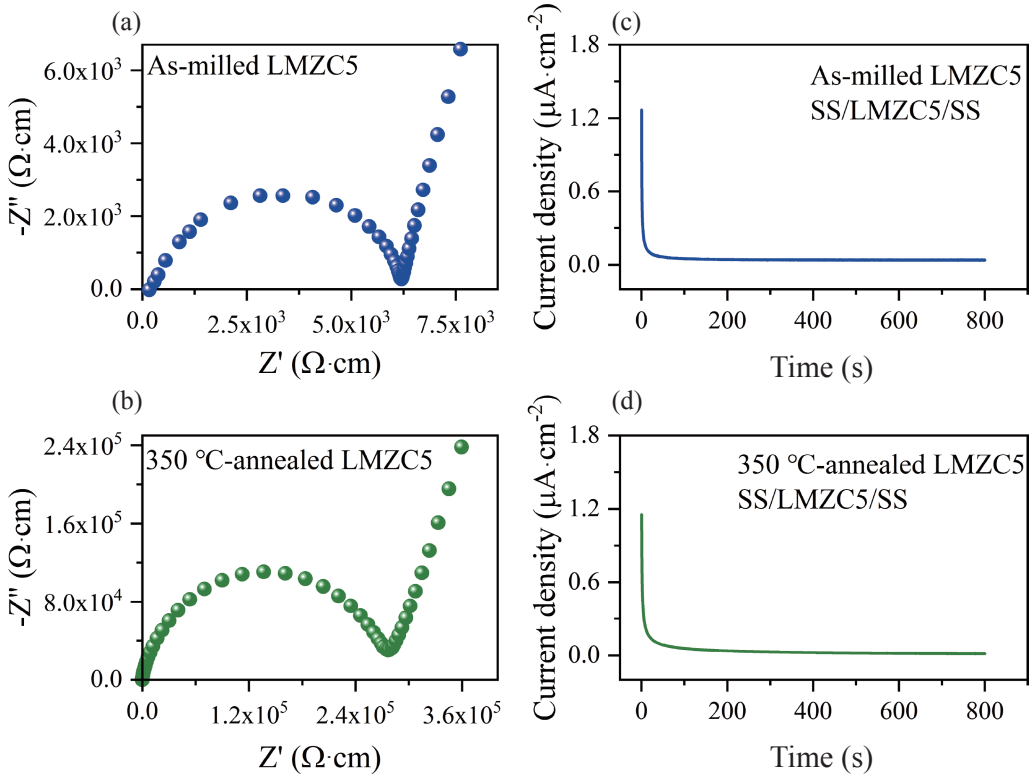

Fig. 3. Conductivity of LMZC5 under different processing conditions. (a, b) Nyquist plots of the as-milled (a) and 350 °C-annealed (b) LMZC5 at 25 °C. (c, d) Chronoamperometry results for the as-milled (c) and 350 °C-annealed (d) LMZC5 at 25 °C with a voltage step of 1 V.

DOI: 10.52396/JUSTC-2022-0071
JUSTC, **2022**, 52(12): 4

Table 1. Conductivities of the as-milled $Li_{2-2x}Mn_{1-x}Zr_xCl_4$ at room temperature.

x in $Li_{2-2x}Mn_{1-x}Zr_xCl_4$	Ionic conductivity ($S·cm^{-1}$)	Electronic conductivity ($S·cm^{-1}$)
0	$1.463×10^{-6}$	$4.191×10^{-9}$
0.1	$1.384×10^{-5}$	$4.949×10^{-9}$
0.2	$2.148×10^{-5}$	$7.097×10^{-9}$
0.3	$6.491×10^{-5}$	$6.534×10^{-9}$
0.4	$9.761×10^{-5}$	$5.476×10^{-9}$
0.5	$1.595×10^{-4}$	$2.552×10^{-9}$
0.6	$6.771×10^{-5}$	$1.197×10^{-9}$

Table 2. Conductivities of the annealed $Li_{2-2x}Mn_{1-x}Zr_xCl_4$ at room temperature.

x in $Li_{2-2x}Mn_{1-x}Zr_xCl_4$	Ionic conductivity ($S·cm^{-1}$)	Electronic conductivity ($S·cm^{-1}$)
0	$2.614×10^{-6}$	$1.299×10^{-9}$
0.1	$1.196×10^{-6}$	$7.093×10^{-9}$
0.2	$1.517×10^{-6}$	$7.131×10^{-9}$
0.3	$2.167×10^{-6}$	$1.932×10^{-9}$
0.4	$2.852×10^{-6}$	$9.270×10^{-10}$
0.5	$3.535×10^{-6}$	$8.454×10^{-10}$
0.6	$3.222×10^{-6}$	$7.501×10^{-10}$

Regardless, a rather high ionic conductivity above 10^{-4} $S·cm^{-1}$ can still be achieved for as-milled LMZC5, so this material should be highly deformable[18].

The electrochemical stability window (ESW) of LMZC5 was calculated by using the established scheme[19–21] based on the Materials Project[22] database. The equilibrium voltage profile and corresponding phase equilibria as a function of applied potential referenced to Li/Li^+ are shown in Fig. 5. The electrochemical reduction originates from Mn^{2+} becoming Mn metal, while the oxidation process originates from the Cl^- anion chemistry with the product of Cl_2. It shows a wide electrochemical window with an oxidation potential of 4.25 V (vs Li/Li^+) and a reduction potential of 2.03 V (vs Li/Li^+).

The ESW predicted above is verified by linear sweep voltammetry (LSV) measurements of all-solid-state Li/Li_6PS_5Cl/LMZC5/LMZC5+C/SS semiblocking cells. The LMZC5+C composite is a mixture of 70 wt% as-milled LMZC5 and 30 wt% carbon. The composite layer is used to improve the electron conduction, thereby making the redox peaks more easily detectable. The LSV results (Fig. 6**)** reveal multiple reduction peaks below 2 V (vs Li/Li^+), along with one oxidation peak above 4 V (vs Li/Li^+), which are consistent with the calculated values. The high Li^+ conductivity, good deformability and high oxidation potential above 4 V make LMZC5 very suitable as a cathode material for ASSLBs.

Finally, the as-milled LMZC5 was integrated as the CAM into an all-solid-state cell. Benefiting from its high ionic conductivity, no solid electrolyte is necessary for the cathode, and electronic conduction in the cathode is fulfilled by electronic conductive agents (CNTs, 30 wt%). The all-solid-state battery uses LIC obtained by 350 °C annealing as the electrolyte. Since its reduction potential is higher than that of the Li-In alloy (0.62 V vs Li/Li^+), a layer of Li_6PS_5Cl is used to separate the negative electrode side to avoid the reaction. The cell was cycled at 0.1 C between 1.5 V and 3.6 V at 25 °C. Mn has various valence states, such as Mn^{2+}, Mn^{3+} and Mn^{4+}. Among $LiMn_{0.5}Zr_{0.5}Cl_4$, if Mn^{2+} rises to Mn^{3+} during charging ($LiMn_{0.5}Zr_{0.5}Cl_4 \leftrightarrow 0.5Li + Li_{0.5}Mn_{0.5}Zr_{0.5}Cl_4$), the theoretical capacity should be 60 $mA·h·g^{-1}$. Meanwhile, referring to the calculated results (Fig. 5**)**, the electrochemical mechanism may also be a conversion reaction ($LiMn_{0.5}Zr_{0.5}Cl_4 + Li \leftrightarrow$

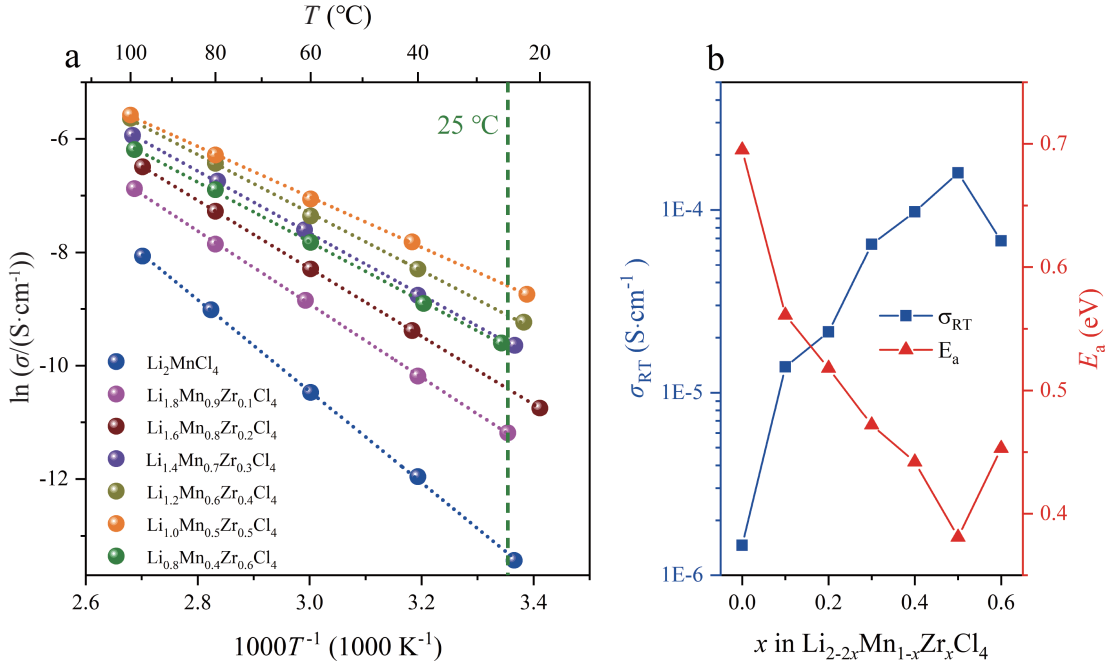

Fig. 4. Conductivity and activation energy evolution upon Zr^{4+} substitution. (a) Arrhenius plots of Li^+ conductivity for as-milled $Li_{2-2x}Mn_{1-x}Zr_xCl_4$. (b) Ionic conductivities at 25 °C and activation energies of as-milled $Li_{2-2x}Mn_{1-x}Zr_xCl_4$.

DOI: 10.52396/JUSTC-2022-0071
JUSTC, **2022**, 52(12): 4

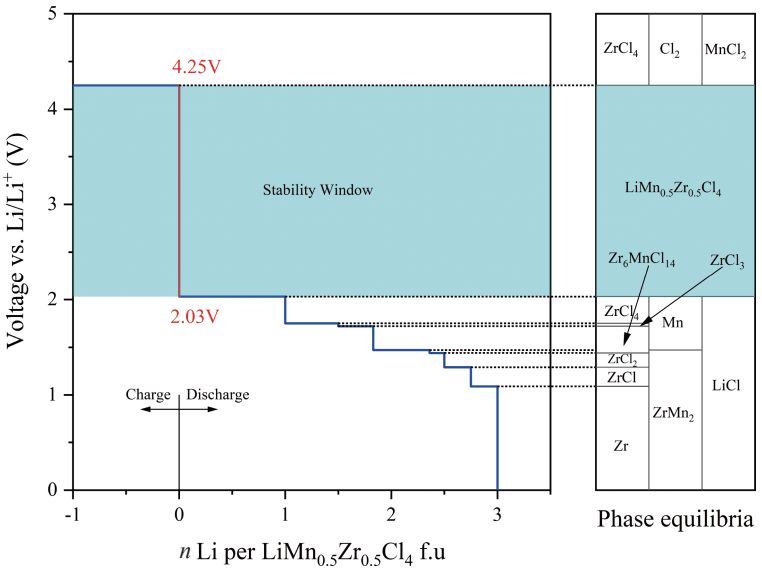

Fig. 5. Thermodynamic equilibrium voltage profiles and the phase equilibria for LMZC5 based on DFT calculations.

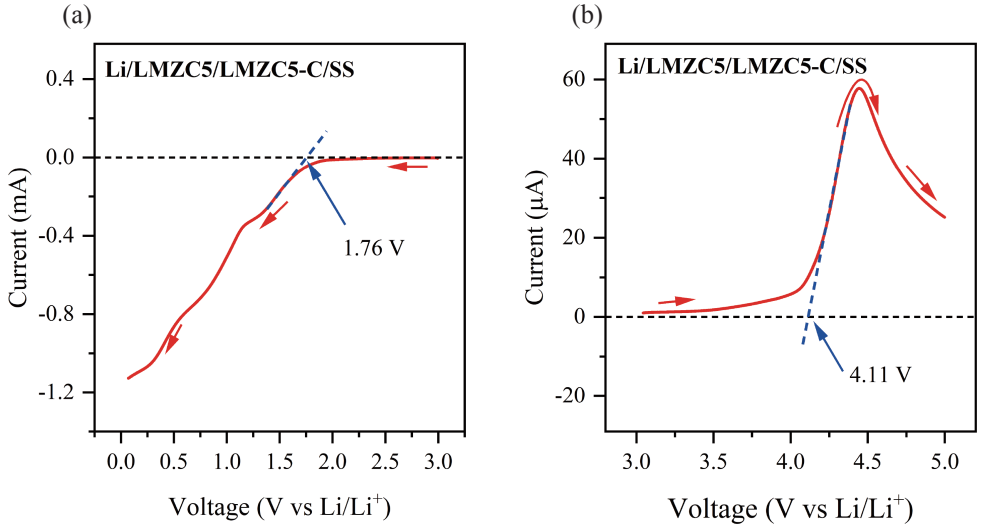

Fig. 6. LSV curves of the Li/Li_6PS_5Cl-LMZC5/LMZC5+C cell at 0.1 mV·s^{-1}. The measurements were conducted at room temperature. (a) 0–3.1 V. (b) 3–5 V.

$2LiCl + 0.5ZrCl_4 + 0.5Mn$), in which case the theoretical capacity should be approximately 121 mA·h·g^{-1}.

The charge-discharge voltage profiles at the 1st, 2nd, 100th, and 200th cycles of the battery are shown in Fig. 7a. The initial charge capacity is extremely low, only 1.6 mA·h·g^{-1}, while the discharge capacity is 52.4 mA·h·g^{-1}. The electrochemical reaction occurred during the discharge process, so it is possible that the cycling takes place through the conversion reaction mentioned above: $LiMn_{0.5}Zr_{0.5}Cl_4 + Li \leftrightarrow 2LiCl + 0.5ZrCl_4 + 0.5Mn$. A voltage plateau appeared at approximately 2.5 V (vs Li/Li^+) with some fluctuations, which may be caused by the decrease in the ionic conductivity affected by the conversion reaction during the discharge process. Given that the discharge capacity reaches only approximately half of the theoretical capacity, there is still an amount of LMZC5 that does not participate in the conversion reaction, which is helpful for ion diffusion in the cathode. The rate capability of the cell is shown in Fig. 7b. Due to the poor cycling stability associated with the conversion reaction, the capacity gradually decreases, especially in the first few cycles. However, upon each increase in the cycling rate, the capacity only dropped slightly; the average capacities at 0.33 C, 0.5 C and 1 C are 22.1 mA·h·g^{-1}, 18.6 mA·h·g^{-1}, and 14.4 mA·h·g^{-1}, respectively. Fig. 7c displays the cycling performance of the cell at a rate of 0.1 C. The cell showed a quick capacity decay during the first few cycles and exhibited considerable cyclability with a reversible discharge capacity of 18 mA·h·g^{-1} after 15 cycles. It maintained a 99.1% Coulombic efficiency and a 14.3 mA·h·g^{-1} discharge capacity after 200 cycles, corresponding to a 79% capacity retention with respect to the fifth cycle. This is the first time that the chloride cathode material has achieved stable and long cycles in an all-solid-state lithium battery, indicating that the development of chloride cathode materials suitable for all-solid-state lithium batteries is a very worthwhile direction to explore.

DOI: 10.52396/JUSTC-2022-0071
JUSTC, **2022**, 52(12): 4

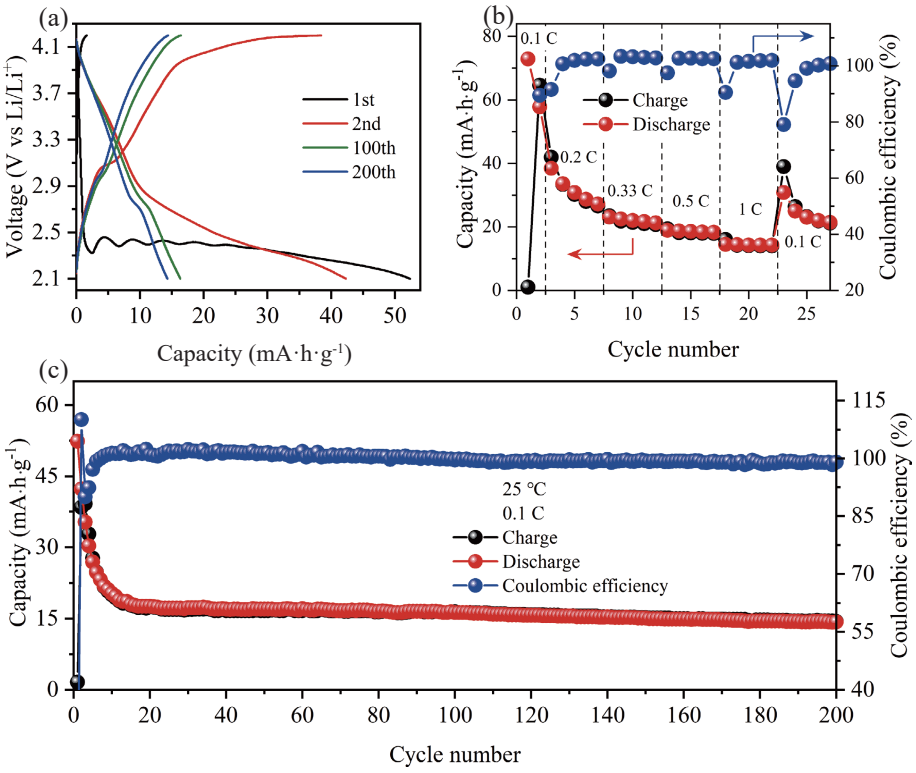

Fig. 7. Electrochemical performance of the Li-In/Li_6PS_5Cl-LIC/LMZC5 cell at 25 °C. (a) Charge and discharge profiles at 0.1 C. (b) Rate performance. (c) Long-term cycling performance at 0.1 C.

To probe the reaction mechanism during cycling, ex situ XRD was conducted on LMZC5 at different depths of discharge, and the results are displayed in Fig. 8. As discharge proceeds, a diffraction peak that does not belong to LMZC5 emerges at approximately 25°, and its intensity keeps increasing with respect to that of LMZC5; at the end of discharge, a significant amount of LMZC5 was still observed, consistent with the low capacities observed in Fig. 7. The additional peak at approximately 25° cannot be indexed to any of the known compounds (including the products speculated by the calculation in Fig. 5), so the specific reaction mechanism cannot be determined. However, the fact that this peak cannot possibly arise from LMZC5 (Fig. 8a) indicates the emergence of new compounds during lithiation. That is, the reaction should follow a conversion mechanism instead of intercalation. It is known that the conversion-type cathode usually has difficulty achieving excellent cycling stability or capacities that are close to the theoretical value, no matter whether the cathode is deformable or not; a typical example is the S cathode in Li-S batteries. This seems to explain why LMZC5 is deformable but still shows poor cycling stability and low capacities.

4 Conclusions

In summary, a series of spinel structure chlorides

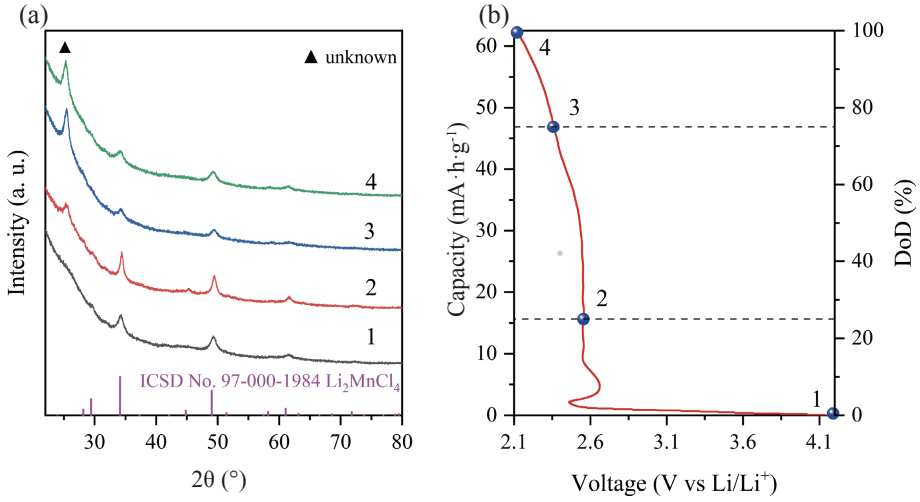

Fig. 8. (a) Ex situ XRD patterns of LMZC5 at different depths of discharge (DoDs). The DoD of each XRD pattern is indicated in (b). (b) The initial discharge profile at 0.1 C, with the DoD for each XRD pattern in (a) indicated.

DOI: 10.52396/JUSTC-2022-0071
JUSTC, **2022**, 52(12): 4

$Li_{2-2x}Mn_{1-x}Zr_xCl_4$ ($0 \leqslant x \leqslant 0.6$) were synthesized successfully by mechanical ball milling and 350 °C annealing. The Li^+ conductivities and electrochemical stabilities of $Li_{2-2x}Mn_{1-x}Zr_xCl_4$ were also investigated. After aliovalent substitution with Zr^{4+}, the Li^+ conductivities of the as-milled samples can be improved to the highest of 0.16 $mS \cdot cm^{-1}$ with the lowest activation energy of 0.381 eV. The ASSLB with LMZC5 cathode active material exhibited excellent cycling stability for 200 cycles at room temperature. Through our study, we have demonstrated the potential possibility of using chlorides with good deformability and high oxidation potential as cathode materials for all-solid-state batteries, which is important to the development of all-solid-state batteries.

Acknowledgements

This work was supported by the National Key R&D Program of China (2018YFA0209600, 2017YFA0208300), the National Natural Science Foundation of China (51802302), and the Fundamental Research Funds for the Central Universities (WK3430000006).

Conflict of interest

The authors declare that they have no conflict of interest.

Biographies

Jipeng Hao is currently a master's student of University of Science and Technology of China (USTC). He received his Bachelor's degree from Southeast University (SEU) in 2019. His main research interests focus on all-solid-state batteries, halide solid state electrolytes and novel cathode active materials.

Cheng Ma received his B.S. degree in Materials Science and Engineering in 2006 from Tsinghua University (Beijing, China) and Ph.D. degree in Materials Science and Engineering in 2012 from Iowa State University. After completing his work as a postdoctoral researcher at the Oak Ridge National Laboratory in 2016, he joined the University of Science and Technology of China as a Professor. His research interests include the critical materials and interfaces in all-solid-state Li batteries.

References

[1] Janek J, Zeier W G. A solid future for battery development. *Nature Energy,* **2016**, *1*: 16141.
[2] Li J, Ma C, Chi M, et al. Solid electrolyte: The key for high-voltage lithium batteries. *Advanced Energy Materials,* **2015**, *5*: 1401408.
[3] Xia S, Wu X, Zhang Z, et al. Practical challenges and future perspectives of all-solid-state lithium-metal batteries. *Chem,* **2019**, *5*: 753–785.
[4] Albertus P, Anandan V, Ban C, et al. Challenges for and pathways toward Li-metal-based all-solid-state batteries. *ACS Energy Letters,* **2021**, *6*: 1399–1404.
[5] Gao X, Liu B, Hu B, et al. Solid-state lithium battery cathodes operating at low pressures. *Joule,* **2022**, *6*: 636–646.
[6] Tanibata N, Kato M, Takimoto S, et al. High formability and fast lithium diffusivity in metastable spinel chloride for rechargeable all-solid-state lithium-ion batteries. *Advanced Energy and Sustainability Research,* **2020**, *1*: 2000025.
[7] Zhao Q, Stalin S, Zhao C Z, et al. Designing solid-state electrolytes for safe, energy-dense batteries. *Nature Reviews Materials,* **2020**, *5*: 229–252.
[8] Nitta N, Wu F, Lee J T, et al. Li-ion battery materials: present and future. *Materials Today,* **2015**, *18*: 252–264.
[9] Ellis B L, Lee K T, Nazar L F. Positive electrode materials for Li-ion and Li-batteries. *Chemistry of Materials,* **2010**, *22*: 691–714.
[10] Cros C, Hanebali L, Latie´ L, et al. Structure, ionic motion and conductivity in some solid-solutions of the LiCl-MCl_2 systems (M=Mg, V, Mn). *Solid State Ionics,* **1983**, *9-10*: 139–147.
[11] Kanno R, Takeda Y, Takada K, et al. Ionic conductivity and phase transition of the spinel system $Li_{2-2x}M_{1+x}Cl_4$ (M=Mg, Mn, Cd). *Journal of The Electrochemical Society,* **1984**, *131*: 469–474.
[12] Han F, Zhu Y, He X, et al. Electrochemical stability of $Li_{10}GeP_2S_{12}$ and $Li_7La_3Zr_2O_{12}$ solid electrolytes. *Advanced Energy Materials,* **2016**, *6*: 1501590.
[13] van Loon C J J, de Jong J. Some chlorides with the inverse spinel structure. *Acta Crystallographica Section B:Structural Science, Crystal Engineering and Materials,* **1975**, *31*: 2549–2550.
[14] Li X N, Liang J W, Luo J, et al. Air-stable Li_3InCl_6 electrolyte with high voltage compatibility for all-solid-state batteries. *Energy & Environmental Science,* **2019**, *12*: 2665–2671.
[15] Liang J, Li X, Wang S, et al. Site-occupation-tuned superionic Li_xScCl_{3+x} halide solid electrolytes for all-solid-state batteries. *Journal of the American Chemical Society,* **2020**, *142*: 7012–7022.
[16] Wang K, Ren Q, Gu Z, et al. A cost-effective and humidity-tolerant chloride solid electrolyte for lithium batteries. *Nature Communications,* **2021**, *12*: 4410.
[17] Kwak H, Han D, Lyoo J, et al. New cost-effective halide solid electrolytes for all-solid-state batteries: Mechanochemically prepared Fe^{3+}-substituted Li_2ZrCl_6. *Advanced Energy Materials,* **2021**, *11*: 2003190.
[18] Asano T, Sakai A, Ouchi S, et al. Solid halide electrolytes with high lithium-ion conductivity for application in 4 V class bulk-type all-solid-state batteries. *Advanced Materials,* **2018**, *30*: 1803075.
[19] Zhu Y Z, He X F, Mo Y F. Origin of outstanding stability in the lithium solid electrolyte materials: insights from thermodynamic analyses based on first-principles calculations. *ACS Applied Materials & Interfaces,* **2015**, *7*: 23685–23693.
[20] Ong S P, Wang L, Kang B, et al. Li−Fe−P−O_2 phase diagram from first principles calculations. *Chemistry of Materials,* **2008**, *20*: 1798–1807.
[21] Mo Y, Ong S P, Ceder G. First principles study of the $Li_{10}GeP_2S_{12}$ lithium super ionic conductor material. *Chemistry of Materials,* **2012**, *24*: 15–17.
[22] Jain A, Ong S P, Hautier G, et al. Commentary: The Materials Project: A materials genome approach to accelerating materials innovation. *APL Materials,* **2013**, *1*: 011002.

DOI: 10.52396/JUSTC-2022-0071
JUSTC, **2022**, 52(12): 4